Physics Letters A 380 (2016) 2300–2306

Contents lists available at ScienceDirect

Physics Letters A

www.elsevier.com/locate/pla

Structural, electronic, and magnetic properties of 3D metal trioxide and tetraoxide superhalogen cluster-doped monolayer BN

Jingjing Meng, Dan Li *, Yuan Niu, Hongmin Zhao, Chunjun Liang, Zhiqun He

Department of Physics, Beijing Jiaotong University, Beijing 1001044, People's Republic of China

ARTICLE INFO

Article history:
Received 23 December 2015
Received in revised form 6 March 2016
Accepted 29 April 2016
Available online 3 May 2016
Communicated by R. Wu

Keywords:
3D metal trioxides and tetraoxide superhalogen cluster
First-principles
Half-metallic
Monolayer BN

ABSTRACT

The structural, electronic, and magnetic properties of monolayer BN doped with 3D metal trioxide and tetraoxide superhalogen clusters are investigated using first-principle calculations. $TMO_{3(4)}$-doped monolayer BN exhibits a low negative formation energy, whereas TM atoms embedded in monolayer BN show a high positive formation energy. $TMO_{3(4)}$ clusters are embedded more easily in monolayer BN than TM atoms. Compared with TMO_3-doped structures, TMO_4-doped structures have a higher structural stability because of their higher binding energies. Given their low negative formation energies, TMO_4-doped structures are more favored for specific applications than TMO_3-doped structures and TM atom-doped structures. Large magnetic moments per supercell and significant ferromagnetic couplings between a TM atom and neighboring B and N atoms on the BN layer were observed in all TMO_4-doped structures, except for TiO_4-doped structures.

1. Introduction

Since the discovery of graphene in 2004 [1], 2D monolayer atomic crystals (i.e., graphene family, 2D chalcogenides, and 2D oxides) have been widely studied because of their unique electronic properties and potential applications in next-generation electronic devices [2–7]. Monolayer BN has also attracted considerable attention because of its chemical stability over graphene [8–11] and has been successfully synthesized in experiments [12–16]. Unlike graphene, BN monolayer is a wide band-gap semiconductor that is favorable for optoelectronic applications. It is also suitable for substrate and gate dielectric for applications in graphene electronics [17–22]. The mobility of the charge carriers in graphene adsorbed on *h*-BN at low temperatures is comparable with that measured in suspended graphene [2,18,19]. For example, we can design the growth of graphene on magnetic monolayer BN substrates as a route for tailoring graphene spin properties [23–27]. Monolayer BN absorbed or doped with nonmagnetic atoms and magnetic transition metal (TM) atoms has been widely investigated. Results show that magnetic moments can be induced easily by nonmagnetic impurities [28,29] and magnetic impurities [30,31] in the semiconducting character BN sheets. Doped monolayer BN with a low formation energy, strong binding energy, and half-metallic ferromagnetic nature is ideal for use in BN-based devices operating at room temperature and above. Given their strong oxidizability and high electronegativity [32], graphene [33] and monolayer MoS_2 [34] doped with magnetic 3D metal trioxide and tetraoxide superhalogen clusters exhibit more stable structures than graphene and monolayer MoS_2 doped with TM atoms.

In this study, we incorporated 3D metal trioxide (TMO_3) and tetraoxide (TMO_4) superhalogen clusters in monolayer BN. The structural, electronic, and magnetic properties of TMO_3 and TMO_4 superhalogen cluster-doped monolayer BN were investigated using first-principle methods based on density functional theory (DFT). Given their negative formation energy and strong binding energy, TMO_4-doped structures are suitable for use in magnetic substrates to induce magnetism in graphene for applications in graphene spin field effect transistors (spin-FETs).

2. Methods

The structural and electronic properties of 3D TM atoms and 3D $TMO_{3(4)}$ superhalogen cluster-doped monolayer BN were calculated utilizing first-principle methods based on spin-polarized DFT. The projector augmented wave potentials [35] and Perdew–Burke–Ernzerhof [36] functional were implemented by the Vienna Ab initio Simulation Package [37]. The wave functions were expanded in plane waves with a kinetic energy cutoff of 500 eV. We employed a 5×5 monolayer BN supercell, where a minimum of 20 Å vacuum spacing was maintained between the adjacent BN layers to eliminate the interaction between them. We employed a *k*-point set generated by an $8 \times 8 \times 1$ Monkhorst–Pack mesh

* Corresponding author.
E-mail addresses: danli@bjtu.edu.cn, lidanyt@163.com (D. Li).

http://dx.doi.org/10.1016/j.physleta.2016.04.042
0375-9601/

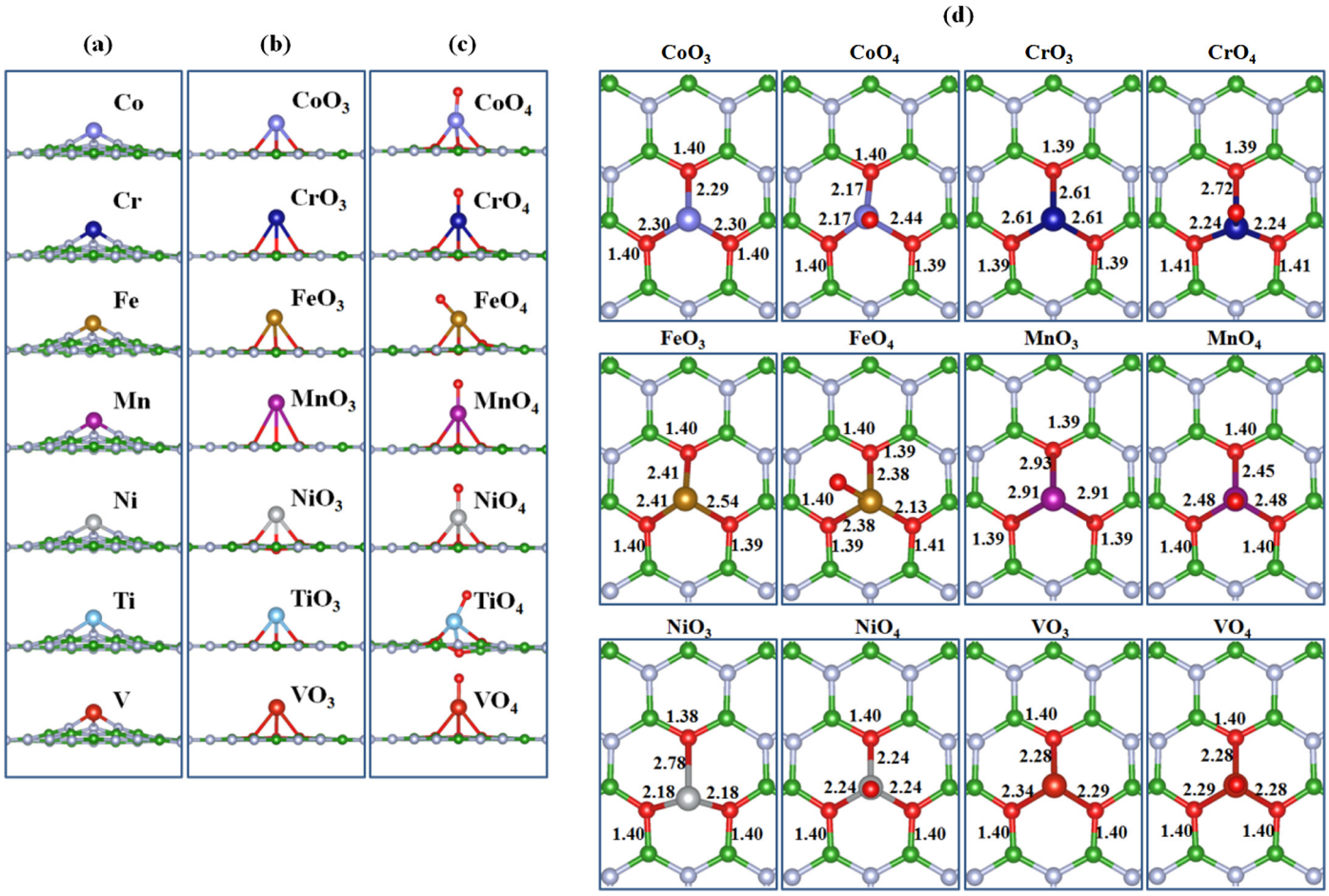

Fig. 1. (Color online.) Side views of atomic structures of (a) TM, (b) TMO_3, and (c) TMO_4 incorporated into monolayer BN. Top views of atomic structures of (d) TMO_3 and TMO_4 incorporated into monolayer BN. The green, gray, red small balls and big balls represent the B, N, O, and dopant, respectively. Bond lengths of TM–O and B–O are shown in Å.

[38]. For partial occupancies, the Gaussian smearing method was adopted. The convergence criterion of our self-consistent calculations for ionic relaxations was 10^{-5} eV between two consecutive steps. All atomic positions and unit cell size were optimized using the conjugate gradient method until the atomic forces were <0.01 eV/Å. Bader analysis was used to calculate charge transfer [39–41].

3. Results and discussions

Different 3D TM atoms (i.e., Co, Cr, Fe, Mn, Ni, Ti, and V) and 3D metal trioxide and tetraoxide superhalogen clusters (i.e., $CoO_{3(4)}$, $CrO_{3(4)}$, $FeO_{3(4)}$, $MnO_{3(4)}$, $NiO_{3(4)}$, $TiO_{3(4)}$, and $VO_{3(4)}$) were incorporated into the monolayer BN for a comprehensive comparison (Fig. 1). In individual TM atom-doped structures, B atoms were substituted by TM atoms. In the $TMO_{3(4)}$-doped structures, B atoms were substituted by TM atoms, and three N atoms around the B atom were substituted by three O atoms. For all doped structures, TM atoms displaced upward from the BN-layer after relaxation. Table 1 and Fig. 2 list the average equatorial and axial bond distances of TM–O and the bond distances of B–O in the $TMO_{3(4)}$-doped structures, the bond distances of TM–N in the TM-doped structures, and the elevation of the TM atoms above the monolayer BN surface for all doped structures. In individual TM atom-doped structures, not only the TM atoms but also the B and N atoms around the TM atoms were significantly displaced upward. Substituted TM atoms with relatively large atomic radii caused local deformation and considerable elevations (1.29–1.79 Å) above the plane of the 2D BN honeycomb structure. The structural parameters of the calculated TM-doped BN sheet are consistent with those in previous studies [30,42]. These results indicate that the

Table 1
Total magnetization of the supercell (μ_{tot}, in μ_B); magnetic moment of TM atoms (μ_{TM}, in μ_B); bond distances of TM–N (d_{TM-N}, in Å), TM–O (equatorial d_{TM-O} and axial d_{TM-O}, in Å), and B–O (d_{B-O}, in Å); and excess charge of TM atoms ($\Delta\rho_{TM}$, in e) and TMO_3 clusters ($\Delta\rho_{TMO_{3(4)}}$, in e) for all TM and $TMO_{3(4)}$ incorporated into monolayer BN.

Dopant	μ_{tot}	μ_{TM}	d_{TM-N}	d_{TM-O}	d_{B-O}	$\Delta\rho_{TM(O_{3(4)})}$
Mn	3.53	3.39	1.84	–	–	−1.25
MnO_3	4.57	4.55	–	2.92	1.39	4.52
MnO_4	4.19	3.93	–	2.47, 1.67	1.40	4.60
Fe	4.41	3.66	1.84	–	–	−1.25
FeO_3	3.45	3.40	–	2.45	1.39	4.51
FeO_4	3.50	3.08	–	2.30, 1.66	1.40	4.60
Co	0.00	0.00	1.76	–	–	−0.91
CoO_3	2.36	2.29	–	2.30	1.40	4.51
CoO_4	2.74	2.18	–	2.26, 1.64	1.40	5.59
Cr	2.67	2.72	1.83	–	–	−1.27
CrO_3	4.74	4.66	–	2.61	1.39	4.50
CrO_4	3.29	3.33	–	2.40, 1.66	1.40	4.55
Ni	0.88	0.63	1.79	–	–	−0.90
NiO_3	1.33	1.26	–	2.38	1.39	4.52
NiO_4	1.85	1.17	–	2.24, 1.65	1.40	4.61
Ti	0.67	0.71	1.88	–	–	−1.34
TiO_3	2.68	2.49	–	2.29	1.40	4.35
TiO_4	0.00	0.00	–	2.19, 1.70	1.43	3.94
V	1.68	1.75	1.85	–	–	−1.31
VO_3	3.66	3.52	–	2.30	1.40	4.43
VO_4	2.30	2.36	–	2.28, 1.65	1.40	4.52